



# CHORUS

This is the accepted manuscript made available via CHORUS. The article has been published as:

## Ferromagnetic resonance phase imaging in spin Hall multilayers

Feng Guo, Jason M. Bartell, and Gregory D. Fuchs

Phys. Rev. B **93**, 144415 — Published 18 April 2016

DOI: [10.1103/PhysRevB.93.144415](https://doi.org/10.1103/PhysRevB.93.144415)

# Ferromagnetic resonance phase imaging in spin Hall multilayers

Feng Guo,<sup>1</sup> Jason M. Bartell,<sup>1</sup> and Gregory D. Fuchs<sup>1,\*</sup>

<sup>1</sup>*School of Applied and Engineering Physics, Cornell University, Ithaca, NY 14853, USA*

We experimentally image the magnetic precession phase of patterned spin Hall multilayer samples to study the rf driving field vector using time-resolved anomalous Nernst effect (TRANE) microscopy. Our ferromagnetic resonance (FMR) measurements quantify the phase and amplitude for both the magnetic precession and the electric current, which allows us to establish the total driving field orientation and the strength of spin Hall effect. In a channel of uniform width, we observe a large spatial variation of the FMR phase laterally across the channel. We interpret our findings in the context of electrical measurement using the spin-transfer torque ferromagnetic resonance technique and show that observed phase variation introduces a systematic correction into the spin Hall efficiency if spatial phase and amplitude variations are not taken into account.

## I. INTRODUCTION

When a spin current traverses the interface between a normal metal and a ferromagnetic metal, it generates a spin-transfer torque<sup>1–3</sup> that efficiently manipulates magnetization. Accurate quantification of current-induced torques is pivotal to first understanding and then engineering spintronic devices for future magnetic memory and information technology. Experimentally, most studies of spin Hall effect (SHE)-driven torques<sup>4–6</sup> have relied on electrical measurements of devices, which are effective because they provide a large signal-to-noise ratio. Typical electrical techniques are spin torque ferromagnetic resonance (ST-FMR)<sup>7–9</sup> for in-plane magnetic moments, and harmonic Hall voltage analysis<sup>10–13</sup> for perpendicularly magnetized devices. An essential assumption of these methods is that both the driving current and the magnetic response are uniform. To gain deeper understanding of SHE-driven torques and go beyond approximate treatments, we quantify the relationship between the driving current and the dynamic magnetic response using phase sensitive magnetic microscopy. Our measurements show that while the assumption of uniform driving current is valid, the assumption of uniform magnetic response is not.

Dynamic magnetic imaging provides a method of characterizing the uniformity of a magnetic response and measuring spin torques. Several techniques have been developed to sense local magnetization dynamics in micro- and nano-structures, including micro-focused Brillouin light scattering (BLS)<sup>14–17</sup>, ferromagnetic resonance force microscopy (FMRFM) dynamics imaging<sup>18–21</sup>, time-resolved magneto-optical Kerr effect (MOKE) microscopy<sup>22,23</sup>, and x-ray magnetic circular dichroism (XMCD)<sup>24–26</sup>. Imaging of phase-resolved propagating spin-waves has been demonstrated using BLS-based technique<sup>27</sup>. Additionally, an optical technique based on polar MOKE for measuring a dc-driven spin-torque vector was recently introduced<sup>28,29</sup>. However, very few phase-sensitive imaging techniques provide a full set of information — a quantitative image of both drive and magnetic response up to gigahertz frequencies.

In this work, we use time-resolved anomalous Nernst

effect (TRANE) microscopy<sup>30,31</sup> to quantify spin Hall efficiency by detecting local ferromagnetic resonance (FMR) precession phase in spin Hall multilayers. By imaging the amplitude and phase of the precessing magnetization in relation to the driving current, we find that the driving field direction in a sample with strong spin torque is different from that in a sample where the spin torque is blocked with a 2 nm thick Hf spacer. More importantly, we demonstrate that even under a uniform driving current, the FMR phase has a large spatial variation, despite the common assumption of quasi-uniformity that is widely applied to the analysis of electrical FMR measurements. In particular, we analyze the consequences of spatial variations in precession phase in the context of device-level measurements such as ST-FMR. We show that for the samples studied in this work, ST-FMR measurements of the spin Hall efficiency has a sizable systematic error.

## II. METHODS

### A. Measurement technique

To simultaneously probe the local magnetic orientation and the rf driving current, we focus 3 ps laser pulses from a Ti:Sapphire laser on the the sample, as illustrated in Fig. 1(a). The vertical component of the transient thermal gradient that is induced by local laser heating generates a voltage pulse corresponding to the magnetization projection in  $y$  direction, through the anomalous Nernst effect (ANE)<sup>32–34</sup>. To excite FMR in our samples, we inject a radio-frequency current  $I_{\text{rf}}$  into the sample, through a circulator, using an arbitrary waveform generator with a fixed frequency of 5.7 GHz. The driving current has a controllable phase, and it is frequency-locked to the stroboscopic repetition rate of the laser pulses, thus enabling measurement of the FMR with a selectable relative phase between the driving current phase and the probe time. Additionally, the increase in the local resistivity due to transient heating produces a voltage corresponding to the stroboscopic time-slice of  $I_{\text{rf}}$ , enabling us to image the local driving current amplitude and phase<sup>31</sup>.

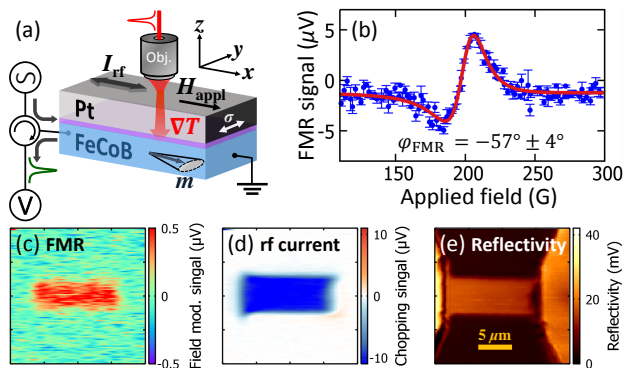


FIG. 1: (a) Schematics of the measurement principle for the time-resolved anomalous Nernst effect (TRANE) microscopy. (b) Example of a ferromagnetic resonance (FMR) spectrum using field modulation. Images measured at a fixed field of 208 G: (c) field modulated FMR signal, (d) rf current with chopping signal and (e) laser reflectivity.

For materials with a large longitudinal spin Seebeck effect (LSSE)<sup>35</sup>, the vertical thermal gradient will also generate a voltage signal proportional to  $m_y$ , if the ferromagnetic layer is interfaced with a spin Hall material (like Pt) because of the inverse spin Hall effect. We point out that although LSSE is indistinguishable from ANE, the presence of LSSE will not affect our results and conclusions.

To perform FMR measurements, an external field is applied along the length of the sample (along  $\hat{x}$ ). The in-plane magnetization component,  $m_y$ , is recorded as a function of applied field. To establish the phase of FMR precession, we fit the signal to  $A(\frac{d\chi'(H)}{dH} \cos \varphi_{\text{FMR}} + \frac{d\chi''(H)}{dH} \sin \varphi_{\text{FMR}})$ , where  $\chi'$  and  $\chi''$  are the real and imaginary dynamic susceptibility functions,  $A$  is the local FMR amplitude, and  $\varphi_{\text{FMR}}$  is the FMR phase at resonance. Fig. 1 (b) shows an example of an FMR spectrum with  $\varphi_{\text{FMR}} = -57^\circ \pm 4^\circ$ . With a fixed magnetic field, we can simultaneously image the FMR signal, the rf current signal, and the laser reflectivity (Figs. 1 (c) - (e), respectively). A more detailed description of the TRANE technique can be found in prior work<sup>31</sup>.

### B. Samples

The samples were dc sputtered on the thermally conductive sapphire substrates and subsequently patterned into a  $5 \mu\text{m} \times 12 \mu\text{m}$  bar geometry using photolithography. For this study, we fabricate samples with a stack structure of  $\text{Fe}_{60}\text{Co}_{20}\text{B}_{20}(4 \text{ nm})/\text{Hf}(t_{\text{Hf}})/\text{Pt}(4 \text{ nm})$ . We use two hafnium thicknesses,  $t_{\text{Hf}}=0.3 \text{ nm}$  and  $t_{\text{Hf}}=2 \text{ nm}$ . The 0.3 nm Hf samples, which we will simply refer to as the “spin torque samples”, present a reasonably large spin torque owing to the spin Hall effect, while maintaining a low damping parameter. From a previous study, a thin Hf spacer layer (near 0.5 nm) is helpful to enhance the spin Hall effect efficiency<sup>36</sup>. In contrast, the samples

with 2 nm thick Hf, or the “non spin torque samples”, have a minimal spin torque. Since the thickness of the Hf spacer already exceeds the spin diffusion length of 1.5 nm in  $\text{Hf}^{12}$ , the Hf layer blocks the spin current flowing from the Pt layer. The spin Hall efficiencies of these two sets of samples are also confirmed with ST-FMR measurements, summarized in Table I. As discussed later, we use the non spin torque sample to establish the local driving field angle in the spin Hall sample via precession phase measurements.

## III. RESULTS AND DISCUSSIONS

### A. FMR phase and driving field angle

First we analyze the effective driving field angle with respect to the sample plane,  $\theta$ , from measurements of the FMR precession phase. In general, the FMR phase  $\varphi_{\text{FMR}}$  simply follows the current phase  $\varphi_{\text{rf}}$  and the driving field angle  $\theta$ . When on resonance,  $\varphi_{\text{FMR}}^\pm = \pm(\varphi_{\text{rf}} + \theta^\pm) - 90^\circ$  with intersection coordinates  $(\varphi_{\text{rf}}^{\text{int}}, \varphi_{\text{FMR}}^{\text{int}}) = (-(\theta^+ + \theta^-)/2, (\theta^+ - \theta^-)/2 - 90^\circ)$ . The superscripts “+” and “-” denote the positive and negative field directions respectively.

We note that there are two torques contributing to the effective driving field: Oersted torque and the spin torque (anti-damping like)<sup>46</sup>. In order to explain the physical meanings of the intersection  $(\varphi_{\text{rf}}^{\text{int}}, \varphi_{\text{FMR}}^{\text{int}})$ , we first discuss the different symmetries between the Oersted driving field and spin torque driving field. As illustrated in Figs. 2 (a) and (b), the Oersted field  $\hat{h}_{\text{Oe}}$  does not change sign when the magnetization reverses, while the spin torque driving field  $\hat{h}_{\text{ST}} = \hat{m} \times \hat{\sigma}$  does. Because of this difference in symmetry between  $\hat{h}_{\text{Oe}}$  and  $\hat{h}_{\text{ST}}$ , the two coordinates  $(\varphi_{\text{rf}}^{\text{int}}, \varphi_{\text{FMR}}^{\text{int}})$  have different physical interpretations.  $-\varphi_{\text{rf}}^{\text{int}}$  is the averaged effective field angle  $\theta_{\text{eff}} = (\theta^+ + \theta^-)/2$ , whereas  $\varphi_{\text{FMR}}^{\text{int}}$  is determined by the difference between  $\theta^+$  and  $\theta^-$ , which is sensitive to the Oersted field orientation. In the Supplementary Information<sup>37</sup> we show that  $\varphi_{\text{rf}}^{\text{int}} \approx -h_{\text{ST}}/h_{\text{Oe}}^\parallel$  and  $\varphi_{\text{FMR}}^{\text{int}} \approx h_{\text{Oe}}^\perp/h_{\text{Oe}}^\parallel - 90^\circ$ , under the assumption of  $h_{\text{ST}}/h_{\text{Oe}}^\parallel$ ,  $h_{\text{Oe}}^\perp/h_{\text{Oe}}^\parallel \ll 1$  ( $h_{\text{Oe}}^\perp$  and  $h_{\text{Oe}}^\parallel$  are the out-of-plane and in-plane components of the Oersted field, respectively).

We only focus on the FMR precession mode that is excited with direct electrical excitation by the spin Hall effect in concert with the Oersted field, consistent with the method used in electrical techniques. Figs. 2 (c) and (d) show the phase dependent rf current and FMR signals, measured at the center of the channel. To investigate the spatial dependence of the phase, we repeat the measurement in Fig. 2 (d) for the top and bottom edges of the channel. The points of intersection  $(\varphi_{\text{rf}}^{\text{int}}, \varphi_{\text{FMR}}^{\text{int}})$  for different positions in the spin torque sample are plotted in Fig. 2 (e). We also include the intersection measured at the center of the non spin torque sample (2 nm Hf spacer) as reference. In the absence of the spin transfer

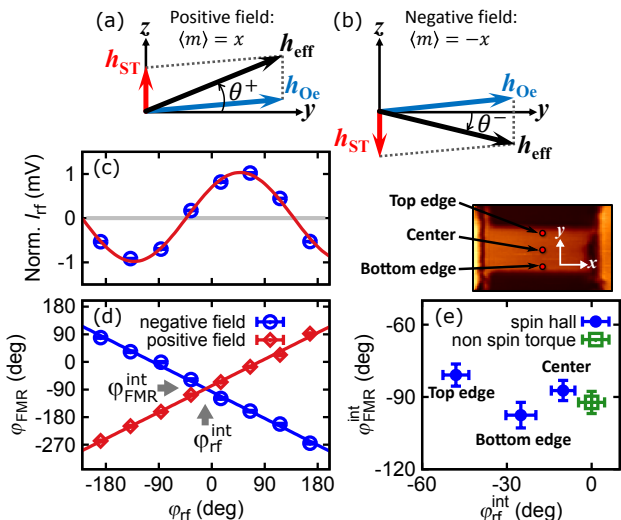


FIG. 2: Diagrams of spin torque field  $h_{ST}$  and Oersted field  $h_{Oe}$  for (a) positive and (b) negative applied fields. The charge current is set to the positive ( $+\hat{x}$ ) for both cases. Normalized current signal (c) and FMR phase (d) as functions of rf current phase, measured at the center of the channel. (e) The points of intersection measured at the top edge, center and bottom edge of the channel. The intersection measured at the center of a non spin torque sample is also included (hollow square) in (e).

torque, only Oersted field is responsible for the effective driving field, and we expect it to be nearly in-plane at the center of the channel. When the spin torque is turned on, given the stack sequence and the positive spin Hall angle for platinum, we expect  $\hat{h}_{ST} \parallel +\hat{z}$ . As a result, the spin torque tilts  $\theta_{eff}$  out of the sample plane, towards the  $+\hat{z}$  direction. As the driving field angle increases,  $\varphi_{rf}^{int}$  will decrease, in agreement with Fig. 2 (e).

### B. Quantification of spin Hall efficiency via phase measurements

Now we quantify spin Hall efficiency by measuring local FMR phases in the middle of the channel for each sample. Because the FMR phase and current phase do not share an absolute reference<sup>37</sup>, we use the non spin torque sample to define the zero current phase, by assuming that the non spin torque sample has an in-plane driving field at the channel center [i.e.  $\varphi_{rf}^{int} = 0$ , see the green point in Fig. 2 (e)]. We also assume that the temporal profiles of both the temperature and thermal gradient remain the same between the two samples, since they have nearly identical structures<sup>47</sup>. Finally, using the FMR phase of the non spin torque sample, we obtain a driving field angle of  $\theta_{eff}^0 = 10.1^\circ \pm 4.2^\circ$  at the center of the spin torque sample, corresponding to a  $(J_s/J_c)^0 = 0.048 \pm 0.020$ . The comparisons between ST-FMR electrical measurements and FMR phase measurements are shown in Table I.

Another important feature of the data is the position

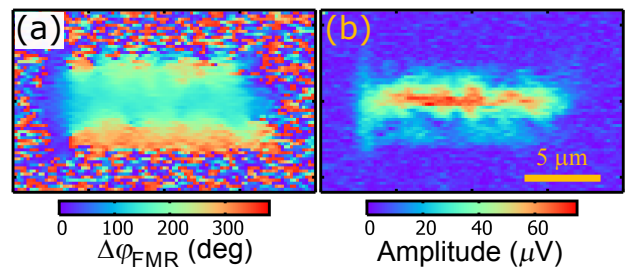


FIG. 3: By fixing  $\varphi_{FMR} = -24^\circ$  and using 6 FMR images at various applied fields, we can decompose (a) the relative FMR phase variation and (b) the FMR amplitude.

dependent FMR phase for the spin torque sample. As shown in Fig. 2 (e),  $\varphi_{rf}^{int}$  near either the top or bottom edge is less than that measured at the center, indicating a larger  $\theta_{eff}$  at the edges. However  $\varphi_{FMR}^{int}$  near either the top or bottom edge shifts towards opposite directions with respect to the center, suggesting a gradual change in  $h_{Oe}^\perp/h_{Oe}^\parallel$ . Furthermore,  $h_{Oe}^\perp$  is expected to be positive at the top edge and negative at the bottom edge, which is consistent with the vertical sequence of the three points in Fig. 2 (e).

### C. FMR phase imaging

Next we demonstrate an approach to image the FMR phase. Instead of recording the FMR spectrum at each location, we combine multiple FMR images to calculate the phase variation. In this example, we fix the rf current phase corresponding to a FMR phase of  $-24^\circ$  at the channel center. We then combine 6 FMR images at various applied fields (from 185 G to 215 G), to reconstruct both phase and amplitude images, shown in Fig. 3 (a) and (b) respectively. The main feature of the phase image is that the phase is quasi-uniform near the center, and it increases near the edges, in quantitative agreement with data in Fig. 2(e) [also see Fig. S1 (a) in Supplemental Information]. The phase variation is more prominent along the  $y$ -direction than that in the  $x$ -direction. In contrast, the FMR amplitude is large near the center and decreases towards either edge, as expected.

Next we speculate on the origin of the phase variation, then we evaluate its influence on global electrical measurements. We point out the precession phase variation is not a result of a nonuniform driving current. Instead, the effective driving field (and thus FMR phase) is not uniform. In a magnetic micro- or nanostructure under a uniform applied field, the internal magnetic field is highly nonuniform near the edges due to the demagnetizing field<sup>38-42</sup>. Similarly, for the rectangular channel structure samples used in this study, the transverse driving field experiences an inhomogeneous demagnetizing field. Consequently the in-plane driving field  $h_{Oe}^\parallel$  inside the ferromagnet<sup>48</sup> has a substantial spatial varia-

tion, which plays an important role in the observed phase variation. In contrast, the out-of-plane  $h_{ST}$  is uniform across the sample given a uniform current density distribution. As a result,  $h_{Oe}^{\parallel}$  is weaker at the channel edges and the effective driving field close to the edges has a larger angle than that at the center, as illustrated in the inset of Fig. 4. We suspect that the spatial variation of the rf driving field is determined by a number of factors, including sample geometries, rf current uniformity, edge properties, and magnetic anisotropy fields. Therefore the details of the phase variations are expected to be sample specific.

#### D. Evaluation of systematic correction in ST-FMR

In the following, we discuss the analysis used in ST-FMR and then we introduce a method to evaluate the systematic correction due to a spatially varying precession mode. The analysis of ST-FMR relies on two assumptions: one is the uniformity of the precession mode and the other is the uniformity of the rf current. Under the macrospin spin approximation, a rectified voltage from ST-FMR is obtained by mixing the rf current with an oscillating magnetoresistance:  $V_{\text{mix}} \propto \theta_p \{ \chi'(H) \cos(\varphi_{\text{rf}} - \varphi_{\text{FMR}}) + \chi''(H) \sin(\varphi_{\text{rf}} - \varphi_{\text{FMR}}) \}$ . By fitting the spectrum  $V_{\text{mix}}(H)$  to a linear combination of the symmetric and anti-symmetric Lorentzian functions, one obtains  $\varphi_{\text{rf}} - \varphi_{\text{FMR}}$  and thus the spin Hall efficiency for the normal metal/ferromagnet combination.

Our results show the measured driving current is uniform, while the assumption of uniform precession breaks down. To understand how observed spatial variations in FMR phase influence ST-FMR measurements, we develop a model to calculate the ST-FMR voltage  $\langle V_{\text{mix}} \rangle$  that includes measured variations in precession amplitude ( $\theta_p$ ) and phase ( $\varphi_{\text{FMR}}$ ). We rewrite the averaged  $\langle V_{\text{mix}} \rangle$  as the integral of the mixing voltage weighted by the precession amplitude ( $\theta_p$ ) (see supplemental material<sup>37</sup> for derivation):

$$\langle V_{\text{mix}} \rangle \propto \chi' \int dr \theta_p(r) \cos[\varphi_{\text{rf}} - \varphi_{\text{FMR}}(r)] + \chi'' \int dr \theta_p(r) \sin[\varphi_{\text{rf}} - \varphi_{\text{FMR}}(r)]. \quad (1)$$

Therefore, we find the equivalent phase difference between the FMR and rf current that would be obtained from the global measurement is:

$$\langle \varphi_{\text{FMR}} - \varphi_{\text{rf}} \rangle = \tan^{-1} \left[ \frac{\int dr \theta_p(r) \sin[\varphi_{\text{FMR}}(r) - \varphi_{\text{rf}}]}{\int dr \theta_p(r) \cos[\varphi_{\text{FMR}}(r) - \varphi_{\text{rf}}]} \right] \quad (2)$$

We can substitute  $\varphi_{\text{FMR}}^0 + \delta\varphi_{\text{FMR}}(r)$  for  $\varphi_{\text{FMR}}$  in Eq. 2 and rewrite to obtain  $\langle \varphi_{\text{FMR}} - \varphi_{\text{rf}} \rangle = \varphi_{\text{FMR}}^0 - \varphi_{\text{rf}} + \Delta$ . The phase correction  $\Delta$  that is determined only by the spatial varying component of the FMR phase variation  $\delta\varphi_{\text{FMR}}(r)$

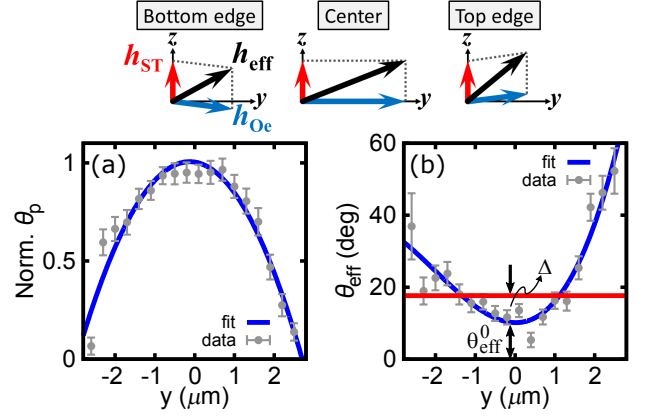


FIG. 4: Top inset: driving field diagrams at various locations of the channel, showing a uniform  $h_{ST}$  and a nonuniform  $h_{Oe}^{\parallel}$ . Spatial distributions of (a) the normalized precession amplitude and (b) effective driving field angle. The blue curves in (a) and (b) are the polynomial fits of the data (gray points). The red line in (b) is the resultant driving field angle that would be obtained from ST-FMR, using Eq. 2.  $\Delta$  is the phase correction discussed in the text.

and the precession amplitude  $\theta_p(r)$ , and is independent of the overall offset  $\varphi_{\text{FMR}}^0$ .

To numerically evaluate the correction resulting from the phase nonuniformity, we use the polynomial fits of the precession amplitude  $\theta_p(y)$  and driving field angle  $\theta_{\text{eff}}(y)$  to mimic the experimental results, plotted in Fig. 4. For simplicity we assume both the phase and amplitude of the precession are uniform in the  $x$  direction and we only consider the spatial variation along the  $y$  direction. We get an “averaged” value of the effective driving field,  $\langle \theta_{\text{eff}} \rangle = \theta_{\text{eff}}^0 + \Delta$ , shown as the red line in Fig. 4 (b). In this example, the phase correction  $\Delta = 7.5^\circ \pm 1.8^\circ$ .

Table I shows the calculated  $\langle J_s/J_c \rangle$ , which accounts for the large spatially varying phase in the spin torque sample, and  $(J_s/J_c)_{\text{ST-FMR}}$  measured directly from ST-FMR. The fact that  $\langle J_s/J_c \rangle$  and  $(J_s/J_c)_{\text{ST-FMR}}$  are consistent validates the previously described method of evaluating ST-FMR result using measured precession profiles and Eq. 2. We note that there is a substantial discrepancy between  $(J_s/J_c)^0$  measured at the channel center and the ST-FMR results. The local value of  $(J_s/J_c)^0$  reflects a more “genuine” spin Hall efficiency since it is least affected by the effect of spatial variation. Thus, we conclude that the ST-FMR technique does not necessarily reflect the phase value (and thus spin Hall efficiency) in the middle of the sample, rather it provides a spatially averaged phase. Although electrical techniques have a superior sensitivity, we show that for our  $5 \mu\text{m}$  wide channels it is essential to include a correction for spatial variations of both precession phase and amplitude to correctly quantify the spin Hall efficiency from electrical measurements.

TABLE I: The spin Hall efficiency,  $(J_s/J_c)_{\text{ST-FMR}}$ , measured with ST-FMR and calculated from the spatial variation of the FMR phase.  $\theta_{\text{eff}}^0$  is the angle of effective driving field at the center, and  $\Delta$  is the phase correction due to the phase variation.  $(J_s/J_c)^0$  is the ratio only at the center, corresponding to  $\theta_{\text{eff}}^0$ ; while  $\langle J_s/J_c \rangle$  is integrated ratio with the phase variation included. The uncertainty of  $\Delta$  is calculated using the standard errors of the polynomial fits in Fig. 4.

Sample	spin torque (0.3 nm Hf)	non spin torque (2 nm Hf)
ST-FMR $(J_s/J_c)_{\text{ST-FMR}} =$	$0.076 \pm 0.002$	$0.010 \pm 0.003$
Phase var. included	$\theta_{\text{eff}}^0 = 10.1^\circ \pm 4.2^\circ$	assume: 0
	$\Delta = 7.5^\circ \pm 1.8^\circ$	$3.4^\circ \pm 1.9^\circ$
	$(J_s/J_c)^0 = 0.048 \pm 0.020$	assume: 0
	$\langle J_s/J_c \rangle = 0.086 \pm 0.031$	$0.015 \pm 0.008$

#### IV. CONCLUSIONS

In summary, we have studied the FMR phase in uniform width spin hall multilayers. Using TRANE microscopy, we have measured the amplitude and phase of both FMR precession and rf driving current, which enables us to determine the angle of driving field vector. In a sample with substantial spin torque, we found that the driving field points to be around  $10^\circ$  out of the sample plane at the center. More importantly, we observed a

substantial precession phase variation across the width of the channel. As a result, for the  $5 \mu\text{m}$  wide samples studied, the spatially integrated spin Hall efficiency is nearly double compared to the efficiency in the middle of the channel. Therefore, although electrical measurements are very effective techniques to quantify the spin Hall effect, we conclude the spatial variations of both precession amplitude and phase can play an important role in the dynamics of confined magnetic structures and should not be overlooked. Finally, we have shown that phase-sensitive imaging is valuable for quantitative studies of the spin Hall effect, and it also provides a general approach for studying precession phase shift induced by the spin-orbit torques recently discussed for various systems<sup>43–45</sup>.

#### ACKNOWLEDGMENTS

The authors thank Daniel C. Ralph and Minh-Hai Nguyen for helpful discussions. This work was supported by AFOSR, under contract No. FA9550-14-1-0243. This work made use of the Cornell Center for Materials Research Shared Facilities which are supported through the NSF MRSEC program (DMR-1120296) as well as the Cornell NanoScale Facility, a member of the National Nanotechnology Coordinated Infrastructure (NNCI), which is supported by the National Science Foundation (Grant ECCS-15420819).

\* Electronic address: [gdf9@cornell.edu](mailto:gdf9@cornell.edu)

- <sup>1</sup> J. C. Slonczewski, J. Magn. Magn. Mater. **159**, L1 (1996).
- <sup>2</sup> L. Berger, Phys. Rev. B **54**, 9353 (1996).
- <sup>3</sup> D. Ralph and M. Stiles, J. Magn. Magn. Mater. **320**, 1190 (2008).
- <sup>4</sup> M. I. Dyakonov and V. I. Perel, Physics Letters A **35**, 459 (1971).
- <sup>5</sup> J. E. Hirsch, Phys. Rev. Lett. **83**, 1834 (1999).
- <sup>6</sup> Y. K. Kato, R. C. Myers, A. C. Gossard, and D. D. Awschalom, Science **306**, 1910 (2004).
- <sup>7</sup> A. A. Tulapurkar, Y. Suzuki, A. Fukushima, H. Kubota, H. Maehara, K. Tsunekawa, D. D. Djayaprawira, N. Watanabe, and S. Yuasa, Nature **438**, 339 (2005).
- <sup>8</sup> J. C. Sankey, P. M. Braganca, A. G. F. Garcia, I. N. Krivorotov, R. A. Buhrman, and D. C. Ralph, Phys. Rev. Lett. **96**, 227601 (2006).
- <sup>9</sup> L. Liu, T. Moriyama, D. C. Ralph, and R. A. Buhrman, Phys. Rev. Lett. **106**, 036601 (2011).
- <sup>10</sup> U. H. Pi, K. Won Kim, J. Y. Bae, S. C. Lee, Y. J. Cho, K. S. Kim, and S. Seo, Applied Physics Letters **97**, 162507 (2010).
- <sup>11</sup> J. Kim, J. Sinha, M. Hayashi, M. Yamanouchi, S. Fukami, T. Suzuki, S. Mitani, and H. Ohno, Nat Mater **12**, 240 (2013).
- <sup>12</sup> C.-F. Pai, M.-H. Nguyen, C. Belvin, L. H. Vilela-Leo, D. C. Ralph, and R. A. Buhrman, Applied Physics Letters **104**, 082407 (2014).
- <sup>13</sup> M. Hayashi, J. Kim, M. Yamanouchi, and H. Ohno, Phys.

- Rev. B **89**, 144425 (2014).
- <sup>14</sup> K. Perzlmaier, M. Buess, C. H. Back, V. E. Demidov, B. Hillebrands, and S. O. Demokritov, Phys. Rev. Lett. **94**, 057202 (2005).
- <sup>15</sup> S. O. Demokritov and V. E. Demidov, Magnetism, IEEE Transactions on **44**, 6 (2008), ISSN 0018-9464.
- <sup>16</sup> V. E. Demidov, M. Buchmeier, K. Rott, P. Krzysteczko, J. Münchenberger, G. Reiss, and S. O. Demokritov, Phys. Rev. Lett. **104**, 217203 (2010).
- <sup>17</sup> H. T. Nembach, J. M. Shaw, T. J. Silva, W. L. Johnson, S. A. Kim, R. D. McMichael, and P. Kabos, Phys. Rev. B **83**, 094427 (2011).
- <sup>18</sup> O. Klein, G. de Loubens, V. V. Naletov, F. Boust, T. Guillet, H. Hurdequint, A. Leksikov, A. N. Slavin, V. S. Tiberkevich, and N. Vukadinovic, Phys. Rev. B **78**, 144410 (2008).
- <sup>19</sup> I. Lee, Y. Obukhov, G. Xiang, A. Hauser, F. Yang, P. Banerjee, D. V. Pelekhov, and P. C. Hammel, Nature **466**, 845 (2010).
- <sup>20</sup> H.-J. Chia, F. Guo, L. M. Belova, and R. D. McMichael, Phys. Rev. Lett. **108**, 087206 (2012).
- <sup>21</sup> F. Guo, L. M. Belova, and R. D. McMichael, Phys. Rev. Lett. **110**, 017601 (2013).
- <sup>22</sup> W. K. Hiebert, A. Stankiewicz, and M. R. Freeman, Phys. Rev. Lett. **79**, 1134 (1997).
- <sup>23</sup> J. P. Park, P. Eames, D. M. Engebretson, J. Berezovsky, and P. A. Crowell, Phys. Rev. Lett. **89**, 277201 (2002).
- <sup>24</sup> S.-B. Choe, Y. Acremann, A. Scholl, A. Bauer, A. Doran,

- J. Sthr, and H. A. Padmore, **304**, 420 (2004).
- <sup>25</sup> M. K. Marcham, P. S. Keatley, A. Neudert, R. J. Hicken, S. A. Cavill, L. R. Shelford, G. van der Laan, N. D. Telling, J. R. Childress, J. A. Katine, et al., *Journal of Applied Physics* **109**, 07 (2011).
- <sup>26</sup> P. Wessels, J. Ewald, M. Wieland, T. Nisius, A. Vogel, J. Viehhaus, G. Meier, T. Wilhein, and M. Drescher, *Phys. Rev. B* **90**, 184417 (2014).
- <sup>27</sup> V. E. Demidov, S. Urazhdin, and S. O. Demokritov, *Applied Physics Letters* **95**, 262509 (2009).
- <sup>28</sup> X. Fan, H. Celik, J. Wu, C. Ni, K.-J. Lee, V. O. Lorenz, and J. Q. Xiao, *Nat Commun* **5**, 3042 (2014).
- <sup>29</sup> X. Fan, A. R. Mellnik, W. Wang, N. Reynolds, T. Wang, H. Celik, V. O. Lorenz, D. C. Ralph, and J. Q. Xiao, *ArXiv e-prints* (2015), 1509.01266.
- <sup>30</sup> J. M. Bartell, D. H. Ngai, Z. Leng, and G. D. Fuchs, *Nat. Commun.* **6**, 8460 (2015).
- <sup>31</sup> F. Guo, J. M. Bartell, D. H. Ngai, and G. D. Fuchs, *Phys. Rev. Applied* **4**, 044004 (2015).
- <sup>32</sup> A. Slachter, F. L. Bakker, and B. J. van Wees, *Phys. Rev. B* **84**, 020412 (2011).
- <sup>33</sup> M. Weiler, M. Althammer, F. D. Czeschka, H. Huebl, M. S. Wagner, M. Opel, I.-M. Imort, G. Reiss, A. Thomas, R. Gross, et al., *Phys. Rev. Lett.* **108**, 106602 (2012).
- <sup>34</sup> A. von Bieren, F. Brandl, D. Grundler, and J.-P. Ansermet, *Applied Physics Letters* **102**, 052408 (2013).
- <sup>35</sup> K.-I. Uchida, H. Adachi, T. Ota, H. Nakayama, S. Maekawa, and E. Saitoh, *Applied Physics Letters* **97**, 172505 (2010).
- <sup>36</sup> M.-H. Nguyen, C.-F. Pai, K. X. Nguyen, D. A. Muller, D. C. Ralph, and R. A. Buhrman, *Applied Physics Letters* **106**, 222402 (2015).
- <sup>37</sup> Supplemental Information (2015).
- <sup>38</sup> J. Jorzick, S. O. Demokritov, B. Hillebrands, M. Bailleul, C. Fermon, K. Y. Guslienko, A. N. Slavin, D. V. Berkov, and N. L. Gorn, *Phys. Rev. Lett.* **88**, 047204 (2002).
- <sup>39</sup> C. Bayer, S. O. Demokritov, B. Hillebrands, and A. N. Slavin, *Applied Physics Letters* **82** (2003).
- <sup>40</sup> C. Bayer, J. P. Park, H. Wang, M. Yan, C. E. Campbell, and P. A. Crowell, *Phys. Rev. B* **69**, 134401 (2004).
- <sup>41</sup> R. D. McMichael and B. B. Maranville, *Phys. Rev. B* **74**, 024424 (2006).
- <sup>42</sup> H. T. Nembach, J. M. Shaw, C. T. Boone, and T. J. Silva, *Phys. Rev. Lett.* **110**, 117201 (2013).
- <sup>43</sup> T. Chiba, G. E. W. Bauer, and S. Takahashi, *Phys. Rev. Applied* **2**, 034003 (2014).
- <sup>44</sup> T. Nan, S. Emori, C. T. Boone, X. Wang, T. M. Oxholm, J. G. Jones, B. M. Howe, G. J. Brown, and N. X. Sun, *Phys. Rev. B* **91**, 214416 (2015).
- <sup>45</sup> W. Zhang, M. B. Jungfleisch, F. Freimuth, W. Jiang, J. Sklenar, J. E. Pearson, J. B. Ketterson, Y. Mokrousov, and A. Hoffmann, *Phys. Rev. B* **92**, 144405 (2015).
- <sup>46</sup> We do not include a field-like spin torque in the discussion since it is indistinguishable from the in-plane Oersted field using phase measurements only.
- <sup>47</sup> We do not expect the extra 1.3 nm Hf in the non spin torque sample to significantly change the temperature and thermal gradient relaxation timescales.
- <sup>48</sup> All the transverse in-plane driving fields in the system will experience such inhomogeneous demagnetizing field, for both in-plane Oersted field ( $h_{Oe}^{\parallel}$ ) and possible field like contribution ( $h_{FL}$ ).